
Corrupted Image Modeling for Self-Supervised Visual Pre-Training

Yuxin Fang^{1*} Li Dong² Hangbo Bao² Xinggang Wang¹ Furu Wei²

Abstract

We introduce **Corrupted Image Modeling (CiM)** for self-supervised visual pre-training. CiM uses an auxiliary generator with a small trainable BEiT to corrupt the input image instead of using artificial mask tokens, where some patches are randomly selected and replaced with plausible alternatives sampled from the BEiT output distribution. Given this corrupted image, an enhancer network learns to either recover all the original image pixels, or predict whether each visual token is replaced by a generator sample or not. The generator and the enhancer are simultaneously trained and synergistically updated. After pre-training, the enhancer can be used as a high-capacity visual encoder for downstream tasks. CiM is a general and flexible visual pre-training framework that is suitable for various network architectures. For the first time, CiM demonstrates that both ViT and CNN can learn rich visual representations using a unified, non-Siamese framework. Experimental results show that our approach achieves compelling results in vision benchmarks, such as ImageNet classification and ADE20K semantic segmentation. For example, 300-epoch CiM pre-trained vanilla ViT-Base/16 and ResNet-50 obtain 83.3 and 80.6 Top-1 fine-tuning accuracy on ImageNet-1K image classification respectively.

1. Introduction

Vision Transformers (ViTs; Dosovitskiy et al., 2020) are transferring the landscape of computer vision, not only in terms of the network architecture design, but also the self-supervised pre-training recipe. Masked image modeling

*Contribution during internship at Microsoft. ¹School of EIC, Huazhong University of Science and Technology ²Microsoft Research. Contact Person: Li Dong <lidong1@microsoft.com>, Xinggang Wang <xgwang@hust.edu.cn>, Furu Wei <fuwei@microsoft.com>.

(MIM; Bao et al., 2021), which randomly masks out some input tokens and then recovers the masked content by conditioning on the visible context, is able to learn rich visual representations and shows promising performance on various vision benchmarks (Zhou et al., 2021; He et al., 2021; Xie et al., 2021; Dong et al., 2021; Wei et al., 2021; El-Nouby et al., 2021).

Originated in masked language modeling (Devlin et al., 2019), MIM (Figure 1a) is tailor-made for specific architectures (Vaswani et al., 2017) as well as input forms, which is generally capable of receiving and processing tokenized inputs such as the artificial mask tokens. Meanwhile, the more common and natural input signal in computer vision is the image in RGB domain with 2D regular grid structures. In order to apply MIM pre-training for images, ViT has to “patchify” the input image into non-overlapping patch embeddings, and then use the special mask tokens to perturb them.

MIM is tightly coupled with the Transformer family, and the use of mask tokens limits its scope of application to some extent. More importantly, MIM is not directly suitable for convolutional neural networks (CNNs; LeCun et al., 1989), the dominant architecture for computer vision in the last decade. Introducing special mask tokens in any intermediate stage of CNN is infeasible, as convolution’s intrinsic dense-sliding-window paradigm brings information leakage between visual features in previous layers. Therefore the large CNN family cannot directly benefit from the upsurge of this new pre-training scheme. Moreover, the use of mask tokens causes a discrepancy between pre-training and fine-tuning, as the artificial mask tokens never appear in the fine-tuning stage.

In this paper, we present a new visual pre-training framework, called **Corrupted Image Modeling (CiM, Figure 1b)**, which avoids directly manipulating mask tokens on pre-trained models and generalizes quite well to both ViT and CNN architectures. Rather than directly using artificial mask tokens to corrupt a portion of non-overlapping patch embeddings as in MIM, CiM uses a small trainable BEiT (Bao et al., 2021) as an auxiliary generator to corrupt the input image. Specifically, the BEiT generator learns to predict visual tokens at the masked positions, where we utilize the predicted distribution to sample tokens’ replacements. The

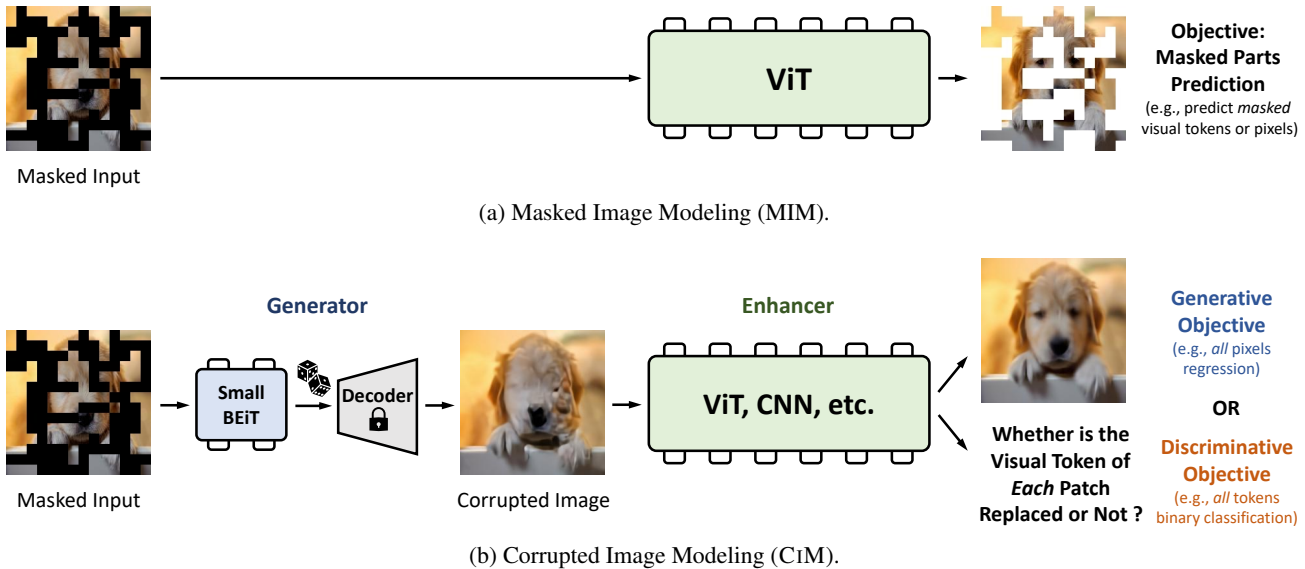


Figure 1. Overview of our Corrupted Image Modeling (CIM) and comparisons with Masked Image Modeling (MIM). MIM (Figure 1a) requires the pre-trained architecture to receive and process the artificial mask tokens, while CIM (Figure 1b) relaxes these restrictions by using a trainable generator to sample corrupted images serving as the input for the enhancer. Similar as BEiT, the small generator learns to predict the golden visual token produced by the pre-trained frozen image tokenizer encoder (not shown in the figure) based on partial observations of the input. The enhancer can be various architectures including CNN and learns either a generative or a discriminative visual pre-training objective. The generator and the enhancer are simultaneously trained and synergistically updated. After pre-training, we throw out the generator and fine-tune the enhancer on downstream tasks. The dice icon in Figure 1b refers to the visual tokens’ stochastic sampling process, and the lock icon means the pre-trained image tokenizer decoder is frozen, *i.e.*, its parameters do not update throughout the pre-training phase.

replaced visual tokens together with the golden tokens produced by a pre-trained frozen image tokenizer encoder (*e.g.*, the DALL-E (Ramesh et al., 2021) dVAE encoder) are then mapped back to the image RGB domain by a pre-trained frozen tokenizer decoder (*e.g.*, the DALL-E dVAE decoder). The resulting corrupted image serves as the input of the enhancer, which is the model to be pre-trained.

For the enhancer, the choice of pre-training objectives is quite flexible. We study two representatives: a generative objective that regresses *all* the original image pixels given the corrupted image (Dosovitskiy et al., 2020), dubbed as **Pixel Residual learning (RESPIX)**, and a discriminative objective that predicts whether *each* visual token is replaced by the small generator or not (Clark et al., 2020), dubbed as **Replaced Visual token Detection (REVDET)**.

Overall, CIM is a novel, general, and flexible pre-training framework suited for different kinds of visual encoders. For the first time, we demonstrate that both ViT and CNN can learn rich visual representations using a unified non-Siamese structure. Moreover, the components of CIM, such as the generator, the image tokenizer (Esser et al., 2021; Yu et al., 2021; Dong et al., 2021), the sampling method (Holtzman et al., 2019), as well as the pre-training objective (Wei et al.,

2021) can be further customized and improved.

After pre-training, the enhancer can be used as a strong feature extractor for various visual downstream tasks. For example, a 300-epoch CIM pre-trained vanilla ViT-Base/16 model can achieve 83.3 Top-1 image classification accuracy when end-to-end fine-tuned on ImageNet-1K. Moreover, we demonstrate that CIM can also easily pre-train high-capacity CNN encoder that generalize well, *e.g.*, a 300-epoch CIM pre-trained vanilla ResNet-50 (He et al., 2016) model achieves 80.6 fine-tuning top-1 accuracy on ImageNet-1K, outperforming all previous results. We also evaluate the transfer learning performance of CIM pre-trained ResNet-50 on the ADE20K semantic segmentation benchmark, and we find that CIM is better than some representative methods based on the Siamese network (Chen & He, 2021) as well as supervised pre-training.

2. Corrupted Image Modeling (CIM)

Figure 1b shows the overview of CIM. Our approach simultaneously learns two neural networks: an auxiliary *generator* and an *enhancer*. The generator is used to corrupt the input image, while the enhancer receives the corrupted



(a) Corrupted image samples from *ImageNet-1K training set*. Although the model is trained using the same dataset, the corrupted image samples still vary to a certain extent. Therefore during pre-training, the generator is able to continuously provide abundant and diverse corrupted samples for the enhancer.



(b) Corrupted image samples from *COCO val split* (Lin et al., 2014) using ImageNet-1K pre-trained model.

Figure 2. Visualizations of some corrupted image samples. For each image set, we show (from left to right) the original image, the masked image, and four different corrupted images sampled from the generator output distribution with the *same* masked input. Simple stochastic sampling can greatly enrich the corrupted image distribution in terms of both low-level features and high-level semantics, which feeds the enhancer better.

image (Figure 2) and learns either a generative or a discriminative visual pretext task. After pre-training, we throw out the generator and fine-tune the enhancer on downstream tasks.

2.1. Generator

Rather than using artificial mask tokens to corrupt the input image, we learn a trainable auxiliary generator to relax the architectural constraints of masked image modeling. Moreover, the generator enriches the diversity of corrupted images via stochastic sampling, which helps the enhancer to generalize. **The generator** consists of a pre-trained frozen image tokenizer, and a small trainable BEiT (Bao et al., 2021).

The frozen image tokenizer in CIM is a pre-trained discrete variational autoencoder (dVAE) (Rolfe, 2016; Van Den Oord et al., 2017), consisting of a paired encoder and decoder. The tokenizer encoder maps the input image into a sequence of discrete visual tokens with a fixed vocabulary size. The tokenizer decoder can recover semantically plausible images given a permutation of appropriate and meaningful visual tokens. We directly use the DALL-E (Ramesh et al., 2021) tokenizer, following BEiT.

The small BEiT consists of several Transformer encoder layers and is trained to perform MIM, which uses two views for each input image, *i.e.*, a sequence of non-overlapping patch embeddings, and their corresponding discrete visual tokens. Patch embeddings are linearly embedded from non-overlapping input image patches. Discrete visual tokens

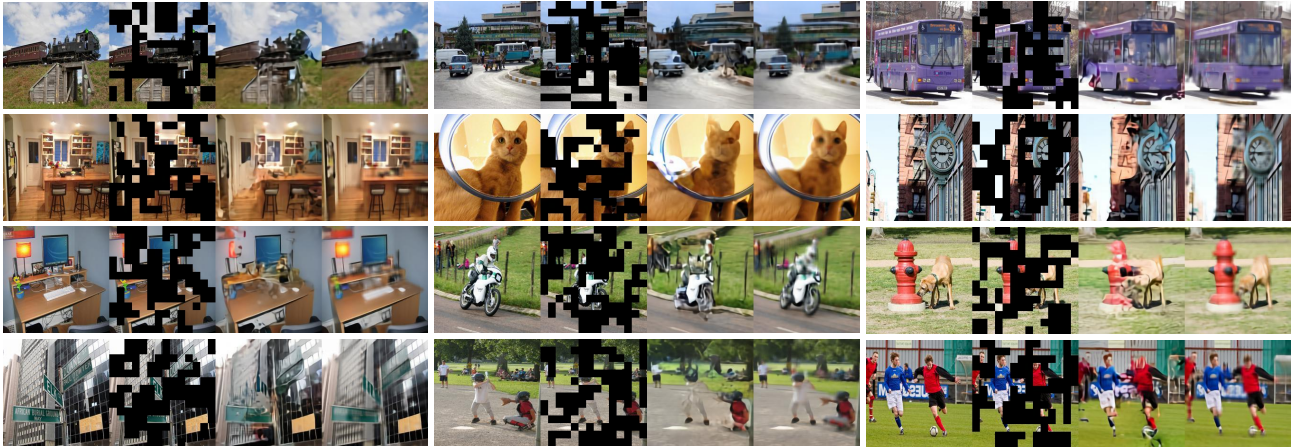
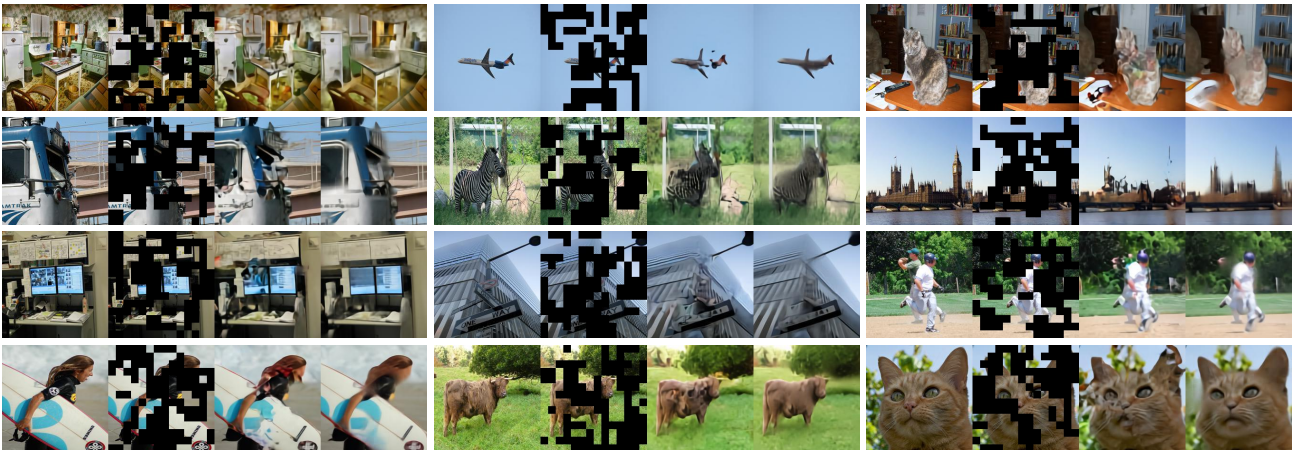
(a) CIM-RESPIX pre-training objective with *sliding window normalized* pixels as the enhancer prediction target.(b) CIM-RESPIX pre-training objective with *unnormalized* pixels as the enhancer prediction target.

Figure 3. Example visualization results on COCO val split images using vanilla ViT-Base/16 model pre-trained with the RESPiX objective using ImageNet-1K training data. For each image quadruplet, we show the original input image (1st column), the masked input image for the generator (2nd column), the corrupted image sampled from the generator output (3rd column), and the enhancer output (4th column). Given the corrupted image, the enhancer is able to perform image denoising, deblurring and completion, *etc.*, and learns to predict plausible output in terms of both low-level features as well as high-level semantics.

are from the DALL-E tokenizer encoder, serving as the prediction target for BEiT.

Given a sequence of patch embeddings, the small BEiT randomly masks out a set of positions. The patch embeddings at the masked positions are replaced with special mask embeddings. The small BEiT takes this corrupted sequence of patch embeddings as the input, and learns to predict the corresponding discrete visual tokens at all masked positions given the visible context only. The size of the small BEiT we use is typically a quarter or a half of the enhancer.

Using discrete visual tokens to represent images enables CIM to perform *stochastic sampling* during the corrupted image’s generation process, which greatly enriches the output set of the generator. In this paper, we directly sample

from softmax with a temperature of 1 at all the masked positions according to the small BEiT output distribution. All the masked tokens are replaced by the sampled visual tokens. The sampled tokens together with the golden tokens that are directly produced by the image tokenizer encoder at all the non-masked positions constitute the input for the image tokenizer decoder. Then the decoder maps those plausible visual tokens to a *corrupted image* (refer to examples in Figure 2), which serves as the input for the enhancer.

2.2. Enhancer

Given the corrupted image sampled from the auxiliary generator, the enhancer learns either a generative or a discriminative visual pretext task. The prediction head is a simple



Figure 4. Normalizations as learning templates for RESPIX. For each image triplet, we visualize the original image (left), the template of using non-overlapping window normalization (He et al., 2021), and the template of the proposed sliding window normalization paradigm. Our approach can provide more accurate and moderate hints that can boost the enhancer’s pre-training as well as improve its representation quantity.

linear layer, and the choice of pre-training objectives is quite flexible. In this paper, we study two representative objectives, coined as **Pixel Residual learning (RESPIX)** and **Replaced Visual token Detection (REVDET)**.

RESPIX (Figure 3) is a generative visual pretext task that requires the enhancer to predict the pixel value for *all* positions given the corrupted input. Instead of directly regressing the original pixel, MAE (He et al., 2021) suggests learning the normalized counterpart. Specifically, the image is partitioned into a set of non-overlapping patches, and each pixel is normalized by the mean and standard deviation of all pixels in the patch it lives in.

In CIM, we further propose to normalize the prediction target inside a *sliding* window, *i.e.*, each pixel is normalized by all pixels in a local 8×8 sized window centered at where the target pixel lives in. We observe improved representation quality using the sliding window normalization paradigm.

Naive pixel recovery without normalization tends to waste modeling capability on learning short-range dependencies and high-frequency details (Ramesh et al., 2021; Bao et al., 2021), while the normalized target can mitigate irrelevant information fittings. From another perspective, normalizations are equal to providing learning templates, as shown in Figure 4. With the normalized prediction target, the enhancer only needs to learn the *residual* pixel value at each position given the normalized pixel value, while the unnormalized target provides no hint therefore the enhancer has to “learn to see in the dark” (*i.e.*, regress from RGB: 0, 0, 0). It is also hard for the enhancer to learn without a template since the corrupted image usually provides bad priors (refer to the corrupted image samples in Figure 2 and Figure 3).

Therefore, we believe appropriate and moderate hints will help the enhancer see better¹.

REVDET is a discriminative visual pretext task that requires the enhancer to determine whether *each* visual token is replaced by a generator sample or not. To be specific, the visual tokens produced by the pre-trained frozen image tokenizer encoder are considered as golden tokens. If a generated visual token is different from the golden token at the same position, that generated token is considered “replaced”, and vice versa.

REVDET is inspired by Clark et al., 2020 in language modeling. The main difference is, in the proposed CIM, the determining criterion of replacement is hidden in the corrupted image. Token replacement is a kind of local, high-frequency operation by nature. However, the visual token set after sampling and replacement is further smoothed and processed by the image tokenizer decoder. Therefore the token sampling and replacement operations are finally embodied as non-local, high-level semantics changes in the corrupted image. The enhancer is required to “decrypt” it and identify all the replaced tokens given the corrupted input, which yields a nontrivial and meaningful visual pretext task². To some extent, REVDET also learns the DALL-E dVAE’s visual codebook similar to BEiT, but in a discriminative manner.

The enhancer is regarded as the visual encoder after pre-training. Moreover, unlike masked image modeling, CIM does not assume too many *architectural priors* for the pre-trained network. We successfully pre-train a high-capacity vanilla ResNet-50 enhancer that achieves compelling transfer learning performance using a similar configuration as pre-training a ViT enhancer. For the first time, we demonstrate that both ViT and CNN can learn strong visual representations using a unified *non-Siamese* framework.

2.3. Training and Optimization

The auxiliary generator and the enhancer are simultaneously trained and synergistically (rather than adversarially as Goodfellow et al., 2014) updated. The trainable part of the generator, *i.e.*, the small BEiT, learns a MIM objective in the same vein as in Bao et al., 2021. Formally, given an input image’s patch embedding sequence $\mathbf{x} = (x_1, \dots, x_n)$, we randomly mask k embeddings at posi-

¹Since there exists information loss in any form of normalization, we have to inject the original image’s information in order to visualize the enhancer output (4th column in Figure 3a). In order to comprehensively demonstrate our method’s behavior, we also include the unnormalized counterpart in Figure 3b for reference, where there is no additional information injection during visualization.

²Therefore, REVDET can be also interpreted as “**Reverse token Detection** from corrupted image”.

tions $\mathbf{m} = (m_1, \dots, m_k)$ using mask token [MASK]³. The resulting masked input sequence $\mathbf{x}^{\text{masked}}$ for BEiT is:

$$\begin{aligned} m_i &\sim \text{uniform}\{1, n\}, \text{ for } i = 1, \dots, k, \\ \mathbf{x}^{\text{masked}} &= \text{replace}(\mathbf{x}, \mathbf{m}, [\text{MASK}]), \end{aligned} \quad (1)$$

where the $\text{replace}(\mathbf{x}, \mathbf{m}, [\text{MASK}])$ operation denotes using the special [MASK] token to replace patch embeddings of \mathbf{x} at positions \mathbf{m} . The small BEiT then encodes $\mathbf{x}^{\text{masked}}$ and learns to maximize $\log p_{\text{BEiT}}(\mathbf{g} | \mathbf{x}^{\text{masked}})$, *i.e.*, the log-likelihood of the golden visual tokens $\mathbf{g} = (g_1, \dots, g_k)$ at the masked positions \mathbf{m} conditioned on $\mathbf{x}^{\text{masked}}$. Notice that the golden tokens are obtained by feeding the original image to the image tokenizer encoder.

In order to generate corrupted image samples $\mathcal{I}^{\text{corrupted}}$ for the enhancer, we sample tokens’ replacements from the BEiT output distribution p_{BEiT} at each masked position j of the encoded $\mathbf{x}^{\text{masked}}$:

$$\begin{aligned} x_j^{\text{sampling}} &\sim p_{\text{BEiT}}(x_j^{\text{sampling}} | \mathbf{x}^{\text{masked}}), \text{ for } j \in \mathbf{m}, \\ \mathbf{x}^{\text{corrupted}} &= \text{replace}(\mathbf{g}, \mathbf{m}, \mathbf{x}^{\text{sampling}}), \end{aligned} \quad (2)$$

where the $\text{replace}(\mathbf{g}, \mathbf{m}, \mathbf{x}^{\text{sampling}})$ operation denotes using the sampled visual token $\mathbf{x}^{\text{sampling}}$ to replace golden tokens of \mathbf{g} at positions \mathbf{m} . Next, the image tokenizer decoder maps $\mathbf{x}^{\text{corrupted}}$ to a corrupted image $\mathcal{I}^{\text{corrupted}}$. The whole image tokenizer is frozen (*i.e.*, not updated throughout the pre-training phase), which directly uses the publicly available⁴ pre-trained DALL-E dVAE weight (Ramesh et al., 2021) following (Bao et al., 2021).

The enhancer takes the corrupted image $\mathcal{I}^{\text{corrupted}}$ as input. For the RESPIX visual pretext task, the enhancer is optimized by a combination of l_1 and l_2 loss for pixel regression. For the REVDet variant, the enhancer is learned by binary cross-entropy loss for replaced visual token detection. The gradients of the enhancer are not back-propagated through the generator.

3. Experiments

3.1. Pre-Training

We study CiM self-supervised pre-trained vanilla ViT-Small/16, vanilla ViT-Base/16 and vanilla ResNet-50 models⁵. We use the actual processed images / views to measure the pre-training epochs (PT epochs; Zhou et al., 2021).

³Typically, we set k equal to 100 \sim 120 given the input sequence length n of 196, *i.e.*, about 50% \sim 60% of the total input patch embeddings are masked out.

⁴<https://github.com/openai/DALL-E>

⁵The vanilla ViT models refer to the design from Dosovitskiy et al., 2020 and Touvron et al., 2021a without further architectural change such as using relative position embeddings and Layer-Scale (Touvron et al., 2021b). The vanilla ResNet-50 model refers to the torchvision ResNet-50 (Paszke et al., 2019) without further architectural change.

Table 1. ImageNet-1K end-to-end fine-tuning top-1 accuracy of vanilla ViT-Small/16 and ViT-Base/16 models.

[†]Doubled attention heads. [‡]Our reproduction.

Models	PT Epochs	Top-1 Acc.
<i>ViT-Small/16 model results</i>		
Scratch (Touvron et al., 2021a)		79.9
MoCo-v3 [†] (Chen et al., 2021b)	600	81.4
DINO (Caron et al., 2021)	1600	81.5
BEiT (Bao et al., 2021)	300	81.3
CiM-RESPIX (Ours)	300	81.5
CiM-REVDet (Ours)	300	81.6
<i>ViT-Base/16 model results</i>		
Scratch (Touvron et al., 2021a)		81.8
Scratch (He et al., 2021)		82.3
DINO (Caron et al., 2021)	1600	82.8
MoCo-v3 (Chen et al., 2021b)	600	83.2
BEiT (Bao et al., 2021)	300	82.9
BEiT (Bao et al., 2021)	800	83.2
MAE [‡] (He et al., 2021)	400	83.1
CiM-REVDet (Ours)	300	83.1
CiM-RESPIX (Ours)	300	83.3

ImageNet-1K (Deng et al., 2009) training data is used to pre-train the small BEiT and the enhancer.

Our pre-training setting generally follows BEiT (Bao et al., 2021). Unlike BEiT, CiM only uses cropping and flipping for data argumentation, while dropout (Srivastava et al., 2014) and stochastic depth (Huang et al., 2016) are not applied. The detailed pre-training settings are summarized in Appendix A.1. Notably, the pre-training configurations are *almost the same* for both ViT and CNN architectures⁶.

In order to evaluate the pre-trained representations from CiM, for both ViT and CNN architectures, we conduct supervised end-to-end fine-tuning experiments on ImageNet-1K image classification in Section 3.2, and ADE20K (Zhou et al., 2019) semantic segmentation in Section 3.3. Ablation study on ImageNet-1K is presented in Section 3.4.

3.2. Image Classification

ViT. The ImageNet-1K end-to-end fine-tuning top-1 accuracy of vanilla ViT-Small/16 and ViT-Base/16 models are presented in Table 1. We fine-tune the small-sized model for 200 epochs, and the base-sized model for 100 epochs. Other self-supervised methods in Table 1 use the same or longer fine-tuning schedule. The fine-tuning hyperparameters mostly follow BEiT, while our layer-wise lr decay rate is set to 0.8 as suggested by Clark et al., 2020. The detailed fine-tuning configurations can be found in Appendix A.2.

As shown in Table 1, compared with other representative

⁶It is expected to achieve better results for ResNet by further tuning, since the pre-training settings from BEiT are originally customized for ViT.

Table 2. ImageNet-1K end-to-end fine-tuning top-1 accuracy of vanilla ResNet-50 model. Methods subscripts indicate the training epochs. RSB (Wightman et al., 2021) is the current vanilla ResNet state-of-the-art training procedure.

[†]Modified ResNet-50 architecture.

Models	PT Epochs	Top-1 Acc.
<i>From-scratch results taken from Wightman et al., 2021</i>		
Original ₉₀ (He et al., 2016)		75.3
PyTorch ₉₀ (Paszke et al., 2019)		76.1
FixRes ₁₂₀ (Touvron et al., 2019)		77.0
DeiT ₃₀₀ (Touvron et al., 2021a)		78.4
ResNet-RS ₃₅₀ [†] (Bello et al., 2021)		78.8
FAMS ₄₀₀ (Dollár et al., 2021)		79.5
<i>Fine-tuning for 100 epochs</i>		
RSB A3 (Wightman et al., 2021)		78.1
CiM-REVDet (Ours)	300	78.6
<i>Fine-tuning for 300 epochs</i>		
RSB A2 (Wightman et al., 2021)		79.8
SimSiam (Chen & He, 2021)	400	79.1
MoCo-v2 (Chen et al., 2020c)	400	79.6
SimCLR (Chen et al., 2020b)	800	79.9
SimCLR (Chen et al., 2020b)	2000	80.0
BYOL (Grill et al., 2020)	400	80.0
SwAV (Caron et al., 2020)	600	80.1
CiM-RESPiX (Ours)	300	79.9
CiM-REVDet (Ours)	300	80.4
<i>Fine-tuning for 600 epochs</i>		
RSB A1 (Wightman et al., 2021)		80.4
CiM-REVDet (Ours)	300	80.6

self-supervised vanilla ViT models, CiM is able to achieve better accuracy with fewer pre-training epochs. Moreover, both REVDet and RESPiX visual pretext task can help the ViT enhancer learn useful representations.

ResNet-50. We demonstrate that CiM can also pre-train a high-capacity ResNet-50 model with the fewest possible modifications from the ViT pre-training settings that can achieve compelling fine-tuning performances on ImageNet-1K. We use the AdamW optimizer (Loshchilov & Hutter, 2017) for fine-tuning, and other configurations basically follow the advanced “training from scratch” recipe of Wightman et al., 2021⁷. For other self-supervised baseline approaches in Table 2, we select the best learning rate out of {5e-3, 8e-3, 12e-3} and keep other settings unchanged. The detailed fine-tuning configurations are given in Appendix A.3.

⁷Despite the advanced training recipe, we believe there exists a better one tailored for *fine-tuning the pre-trained ResNet*. For example, a recent work (Liu et al., 2022) reports that pre-trained CNN can also benefit from layer-wise learning rate decay when fine-tuned on downstream tasks. We also observe performance gains in some ResNet fine-tuning preliminary trials using layer-wise lr decay. Detailed results will be reported in the future.

Table 3. ADE20K semantic segmentation performances (mIoU) of ViT and ResNet-50 models.

Models	PT Epochs	Top-1 Acc.
<i>Fine-tuning for 160k iterations</i>		
DINO (Caron et al., 2021)	1600	43.0
BEiT (Bao et al., 2021)	300	43.2
CiM-RESPiX (Ours)	300	43.5

(a) Vanilla ViT-Base/16 as encoder with one linear layer as decoder.

Models	PT Epochs	mIoU
<i>Fine-tuning for 80k iterations</i>		
Training from Scratch		
IN1K Supervised [†] (He et al., 2019)	120	35.9
CiM-REVDet (Ours)	300	36.2
<i>Fine-tuning for 160k iterations</i>		
Training from Scratch		
IN1K Supervised [†] (He et al., 2019)	120	36.1
BYOL (Grill et al., 2020)	400	37.1
SimSiam (Chen & He, 2021)	400	37.1
SwAV (Caron et al., 2020)	600	37.2
MoCo-v2 (Chen et al., 2020c)	400	37.5
SimCLR (Chen et al., 2020b)	800	37.6
SimCLR (Chen et al., 2020b)	2000	37.7
CiM-REVDet (Ours)	300	38.0

(b) Vanilla ResNet-50 as encoder with a classic FCN as decoder.

[†]Modified ResNet-50 architecture.

As shown in Table 2, Under such a demanding training procedure, we find the CiM pre-trained ResNet-50 model can outperform several representative self-supervised methods based on the Siamese framework as well as the modernized state-of-the-art ResNet-50 results. Using the same fine-tuning recipe, we also observe performance degeneration for some baseline self-supervised representations compared with the RSB from scratch results. Notably, even with the extreme 600-epoch training schedule, the CiM representation can still improve the RSB A1 performance by 0.2%.

Different from ViT, we find CiM pre-trained ResNet-50 works better with the REVDet visual pretext task, which indicates that the pretext task can be further customized and improved for different architectures.

3.3. Semantic Segmentation

We study the transfer learning performance of CiM pre-trained vanilla ViT-Base/16 and ResNet-50 models on the challenging ADE20K semantic segmentation benchmark. The pre-trained models are used as an encoder, and we purposefully choose a simple decoder to better evaluate the pre-trained representations. Experiments are conducted with the code base of Bao et al., 2021 and MMSegmentation, 2020.

Specifically, for ViT-Base/16 we use a simple linear layer as the decoder, and for ResNet-50 we choose the commonly

Table 4. Ablation study: masking strategy and masking ratio.

Masking Strategy	Masking Ratio	Top-1 Acc.
Blockwise	40%	82.8
Blockwise	50%	82.9
Blockwise	60%	82.8
Random	40%	83.0
Random	50%	83.3
Random	60%	83.1

used FCN (Long et al., 2015) as the decoder. For ViT, the baseline settings as well as the fine-tuning recipes are from Bao et al., 2021. We select the best learning rate out of $\{1e-4, 3e-4, 5e-4, 7e-4\}$ for DINO. For BEiT we use the default setting (lr $7e-4$ with a decay rate of 0.65). For CiM pre-trained ViT, we set the fine-tuning lr equal to $3e-4$ with a decay rate of 0.8 as suggested by Clark et al., 2020. For ResNet-50, we use the classic configuration⁸ for all methods, *i.e.*, the optimizer is SGD with momentum 0.9, the peak learning rate is 0.01 with a poly decay schedule, and the batch size is 16. The training crop size is set to 512 for all models, and we use single-scale inference.

As summarized in Table 3, when transferred to semantic segmentation task, CiM pre-trained models can still achieve competitive performances compared with other approaches. Notably, for ResNet-50, as the fine-tuning schedule becomes longer (*i.e.*, 80k iterations \rightarrow 160k iterations), the performance gain from the ImageNet-1K supervised pre-trained representation is small. Moreover, the performance is even worse than training from scratch. Meanwhile, the CiM pre-trained ResNet-50 representation can provide sustaining performance gain for a longer fine-tuning schedule.

Together with the observation from Section 3.2, we demonstrate CiM is a unified and flexible *non-Siamese* framework that is capable of pre-training both strong ViT and CNN visual encoders.

3.4. Ablation Studies

Ablation studies are conducted using 300-epoch CiM-RESPIX pre-trained ViT-Base model with 100 epochs fine-tuning on ImageNet-1K unless specified.

Masking Strategy and Masking Ratio. As shown in Table 4, we observe CiM works better with simple random masking (He et al., 2021; Xie et al., 2021) compared with the blockwise masking strategy proposed in BEiT.

The optimal random masking ratio is around 50%, which we find also holds for the REVDet pretext task, in part because it provides almost equal amounts of positive and negative

⁸https://github.com/open-mmlab/mmdetection/blob/master/configs/fcn/fcn_r50-d8_512x512_160k_ade20k.py

Table 5. Ablation study: depth of the small BEiT in the generator and weight sharing[†].

[†]Sharing the patch embedding linear layer and the first 2 Transformer encoder layers between the small BEiT and the enhancer.

# Encoder Layers	Weight Sharing	Top-1 Acc.
4	✗	83.1
4	✓	83.3
5	✓	83.2
6	✓	83.2
7	✓	83.1

Table 6. Ablation study: pixel reconstruction target for RESPIX pre-training objective. “Norm. with non-overlap window” is proposed in (He et al., 2021).

RESPIX Reconstruction Target	Top-1 Acc.
Without normalization	82.8
Norm. with non-overlap window	83.0
Norm. with sliding window	83.3

training samples.

The Small BEiT Depth and Weight Sharing. Following (Meng et al., 2021; Chi et al., 2021), we adjust the size of the small trainable BEiT by varying its depth (the number of Transformer encoder layers). As summarized in Table 5, BEiT with 4 to 6 layers is generally fine.

It is also beneficial to share the patch embedding layer as well as the first two Transformer encoder layers between the small BEiT and enhancer as long as the enhancer is also ViT. We hypothesize that sharing the earlier layers can help calibrate the enhancer, since the small BEiT receives the real inputs while the enhancer sees the same sources but with corrupted views.

Target for RESPIX. We believe an appropriate normalization technique can provide moderate hints that can help improve the enhancer’s representation quality with the RESPIX visual pretext task (see our discussion of Figure 4). As shown in Table 6, the proposed sliding window normalization improves the fine-tuning accuracy by 0.5% *vs.* the reconstruction target without normalization, and is also 0.3% better than the normalization method proposed in (He et al., 2021).

Sampling Strategy for Visual Tokens. Using discrete visual tokens to represent images enables CiM to use stochastic sampling techniques during the corrupted image’s generation process, which can greatly enrich the output set of the generator and help the enhancer generalize well. For masked image modeling, randomly masking out a portion of patch embeddings can help regularize the pre-training, while for our approach, regularization for the enhancer mainly comes

Table 7. Ablation study: sampling strategy for visual tokens. “ \times ” denotes that the training is diverged.

[†]Sample the token with the largest likelihood. [‡]Sample from softmax .

Sampling Strategy	Top-1 Acc.
Uniform sampling	\times
argmax sampling [†]	\times
Gumbel sampling [‡]	83.3

from the diversity of the corrupted images, therefore tricks like dropout and stochastic depth are not used in CiM.

As presented in Table 7, the image visual token representation with stochastic sampling from the generator is crucial for CiM. In contrast, we find that uniform sampling from the codebook of the image tokenizer and argmax sampling cannot pre-train the enhancer as expected.

Image Corrupting Strategy for ResNet-50. In Table 8, we demonstrate that it is crucial to use the generator with a trainable BEiT to corrupt images in order to successfully pre-train CNN with the proposed CiM. We experiment with another generative visual pretext task for ResNet-50 pre-training, *i.e.*, using 50% random erasing (Zhong et al., 2020) to corrupt the input image, and the model is required to recover the erased pixels based on the visible context. We find this pretext task fails to transfer.

The image corrupting process of CiM still has room for improvement. For example, the image tokenizer encoder-decoder pair plays an essential role in the image generation process, which determines the characteristics and styles of the corrupted image distribution. Therefore it has a big impact on the representation quality of the enhancer. In this paper, we directly use the same image tokenizer as BEiT for a fair and clear comparison with recent works. Meanwhile, we believe other image tokenizers, such as (Esser et al., 2021; Dong et al., 2021; Yu et al., 2021), deserve an in-depth study for CiM pre-training in the future.

4. Related Work

Image Restoration is the operation of taking a corrupted, noisy image and estimating the clean, original image. Representative learning-based approaches (Dong et al., 2015; Zhang et al., 2017b; Chen et al., 2021a) are optimized via establishing mappings between corrupted and original images from large-scale paired datasets. The corrupted images are usually generated from hand-crafted degradation transformations given the original images. In our CiM framework, the corrupted images are sampled from a trainable BEiT’s output distribution, we observe not only the low-level image features are degenerated, but also the high-level semantics are affected. Therefore our method can provide abundant nontrivial image pairs feeding the enhancer.

Table 8. Ablation study: image corrupting strategy for vanilla ResNet-50 pre-training. “ \times ” denotes the training is diverged.

Image Corrupting Strategy	Top-1 Acc.
50% Random Erasing (Zhong et al., 2020) Generator in CiM	\times 80.6

Siamese Framework is the dominating self-supervised visual pre-training approach over the past few years, which typically relies on strong hand-crafted data augmentations to generate different views of the same image and learns in a contrastive manner. To maintain a large and informative negative sample set, memory banks (He et al., 2020) or large batch size (Chen et al., 2020b) is used. Follow-up works (Grill et al., 2020; Chen & He, 2021) further eliminate the requirement of using negative samples. Caron et al. (2021) and Chen et al. (2021b) study the vanilla ViT self-supervised visual pre-training within Siamese frameworks.

Masked Image Modeling (MIM) learns rich visual representations via masked parts prediction by conditioning on visible context. ViT (Dosovitskiy et al., 2020) and iGPT (Chen et al., 2020a) report the first meaningful MIM visual pre-training results. BEiT (Bao et al., 2021) greatly improves MIM’s performance via masked visual token prediction, and PeCo (Dong et al., 2021) finds injecting perceptual similarity during visual codebook learning benefits MIM pre-trained representation. He et al. (2021) and Xie et al. (2021) re-explore pixel regression in MIM. Zhou et al. (2021) and El-Nouby et al. (2021) incorporate MIM within Siamese frameworks. MaskFeat (Wei et al., 2021) proposes to predict hand-crafted image feature descriptors at the masked positions. As MIM is originated in masked language modeling (Devlin et al., 2019), CiM is inspired by (Clark et al., 2020). In our CiM, visual-token-based MIM plays an important role during the corrupted image generation process, as the stochastic sampling ability greatly enriches the corrupted image set.

5. Limitations and Future Research

In this paper, we focus more on the architectural flexibility and universality of CiM, while the scaling behavior is not fully explored. The image tokenizer we use is essentially a large CNN and adds nontrivial overhead during pre-training, we believe that it can be largely resolved by using a more advanced tokenizer, such as ViT-VQGAN (Yu et al., 2021), which reports much higher throughput and better generation quality. Moreover, the influence of corrupted images’ characteristics, styles and distributions on the pre-trained representation quality still needs more investigation. For CNN models, an even better pre-training and fine-tuning recipe remains to be explored. We also would like to apply the proposed method to various vision architectures other

than ViT or CNN. In addition, despite the generative and discriminative objectives explored in the paper, other advanced pre-training objectives, such as corrupted feature prediction (Wei et al., 2021), can be applicable to our CiM.

6. Conclusion

We introduce a strong, flexible and unified self-supervised visual pre-training framework with few architectural constraints for the model to be pre-trained. Unlike the mainstream Siamese pre-training frameworks based on strong artificial data augmentations as well as masked image modeling pre-training relying on randomly inserting artificial mask tokens to input embeddings, our CiM pre-trained encoder learns from the corrupted view generated from a trainable neural network’s output distribution. Given the stochastic sampling ability, CiM defends using discrete visual token representations during pre-training to some extent. Experimental results show that the proposed approach achieves competitive pre-training performance for both vision Transformers and convolutional neural networks.

Acknowledgement

We would like to acknowledge Yaru Hao for the helpful discussions.

References

- Bao, H., Dong, L., and Wei, F. BEiT: BERT pre-training of image transformers. *arXiv preprint arXiv:2106.08254*, 2021.
- Bello, I., Fedus, W., Du, X., Cubuk, E. D., Srinivas, A., Lin, T.-Y., Shlens, J., and Zoph, B. Revisiting resnets: Improved training and scaling strategies. *arXiv preprint arXiv:2103.07579*, 2021.
- Berman, M., Jégou, H., Vedaldi, A., Kokkinos, I., and Douze, M. Multigrain: a unified image embedding for classes and instances. *arXiv preprint arXiv:1902.05509*, 2019.
- Caron, M., Misra, I., Mairal, J., Goyal, P., Bojanowski, P., and Joulin, A. Unsupervised learning of visual features by contrasting cluster assignments. *arXiv preprint arXiv:2006.09882*, 2020.
- Caron, M., Touvron, H., Misra, I., Jégou, H., Mairal, J., Bojanowski, P., and Joulin, A. Emerging properties in self-supervised vision transformers. *arXiv preprint arXiv:2104.14294*, 2021.
- Chen, H., Wang, Y., Guo, T., Xu, C., Deng, Y., Liu, Z., Ma, S., Xu, C., Xu, C., and Gao, W. Pre-trained image processing transformer. In *CVPR*, 2021a.
- Chen, M., Radford, A., Child, R., Wu, J., Jun, H., Luan, D., and Sutskever, I. Generative pretraining from pixels. In *ICML*, 2020a.
- Chen, T., Kornblith, S., Norouzi, M., and Hinton, G. A simple framework for contrastive learning of visual representations. In *ICML*, 2020b.
- Chen, X. and He, K. Exploring simple siamese representation learning. In *CVPR*, 2021.
- Chen, X., Fan, H., Girshick, R., and He, K. Improved baselines with momentum contrastive learning. *arXiv preprint arXiv:2003.04297*, 2020c.
- Chen, X., Xie, S., and He, K. An empirical study of training self-supervised vision transformers. *arXiv preprint arXiv:2104.02057*, 2021b.
- Chi, Z., Huang, S., Dong, L., Ma, S., Singhal, S., Bajaj, P., Song, X., and Wei, F. Xlm-e: cross-lingual language model pre-training via electra. *arXiv preprint arXiv:2106.16138*, 2021.
- Clark, K., Luong, M.-T., Le, Q. V., and Manning, C. D. Electra: Pre-training text encoders as discriminators rather than generators. *arXiv preprint arXiv:2003.10555*, 2020.
- Cubuk, E. D., Zoph, B., Shlens, J., and Le, Q. V. Randaugment: Practical automated data augmentation with a reduced search space. In *Proceedings of the IEEE/CVF Conference on Computer Vision and Pattern Recognition Workshops*, pp. 702–703, 2020.
- Deng, J., Dong, W., Socher, R., Li, L.-J., Li, K., and Fei-Fei, L. Imagenet: A large-scale hierarchical image database. In *CVPR*, 2009.
- Devlin, J., Chang, M.-W., Lee, K., and Toutanova, K. BERT: Pre-training of deep bidirectional transformers for language understanding. In *NAACL*, 2019.
- Dollár, P., Singh, M., and Girshick, R. Fast and accurate model scaling. In *CVPR*, 2021.
- Dong, C., Loy, C. C., He, K., and Tang, X. Image super-resolution using deep convolutional networks. *TPAMI*, 2015.
- Dong, X., Bao, J., Zhang, T., Chen, D., Zhang, W., Yuan, L., Chen, D., Wen, F., and Yu, N. Peco: Perceptual codebook for bert pre-training of vision transformers. *arXiv preprint arXiv:2111.12710*, 2021.
- Dosovitskiy, A., Beyer, L., Kolesnikov, A., Weissenborn, D., Zhai, X., Unterthiner, T., Dehghani, M., Minderer, M., Heigold, G., Gelly, S., et al. An image is worth 16x16 words: Transformers for image recognition at scale. *arXiv preprint arXiv:2010.11929*, 2020.

- El-Nouby, A., Izacard, G., Touvron, H., Laptev, I., Jegou, H., and Grave, E. Are large-scale datasets necessary for self-supervised pre-training? *arXiv preprint arXiv:2112.10740*, 2021.
- Esser, P., Rombach, R., and Ommer, B. Taming transformers for high-resolution image synthesis. In *CVPR*, 2021.
- Goodfellow, I., Pouget-Abadie, J., Mirza, M., Xu, B., Warde-Farley, D., Ozair, S., Courville, A., and Bengio, Y. Generative adversarial nets. In *NeurIPS*, 2014.
- Grill, J.-B., Strub, F., Altché, F., Tallec, C., Richemond, P. H., Buchatskaya, E., Doersch, C., Pires, B. A., Guo, Z. D., Azar, M. G., et al. Bootstrap your own latent: A new approach to self-supervised learning. *arXiv preprint arXiv:2006.07733*, 2020.
- He, K., Zhang, X., Ren, S., and Sun, J. Deep residual learning for image recognition. In *CVPR*, 2016.
- He, K., Fan, H., Wu, Y., Xie, S., and Girshick, R. Momentum contrast for unsupervised visual representation learning. In *CVPR*, 2020.
- He, K., Chen, X., Xie, S., Li, Y., Dollár, P., and Girshick, R. Masked autoencoders are scalable vision learners. *arXiv preprint arXiv:2111.06377*, 2021.
- He, T., Zhang, Z., Zhang, H., Zhang, Z., Xie, J., and Li, M. Bag of tricks for image classification with convolutional neural networks. In *CVPR*, 2019.
- Hoffer, E., Ben-Nun, T., Hubara, I., Giladi, N., Hoefler, T., and Soudry, D. Augment your batch: better training with larger batches. *arXiv preprint arXiv:1901.09335*, 2019.
- Holtzman, A., Buys, J., Du, L., Forbes, M., and Choi, Y. The curious case of neural text degeneration. *arXiv preprint arXiv:1904.09751*, 2019.
- Huang, G., Sun, Y., Liu, Z., Sedra, D., and Weinberger, K. Q. Deep networks with stochastic depth. In *ECCV*, 2016.
- LeCun, Y., Boser, B., Denker, J. S., Henderson, D., Howard, R. E., Hubbard, W., and Jackel, L. D. Backpropagation applied to handwritten zip code recognition. *Neural computation*, 1989.
- Lin, T.-Y., Maire, M., Belongie, S., Hays, J., Perona, P., Ramanan, D., Dollár, P., and Zitnick, C. L. Microsoft coco: Common objects in context. In *ECCV*, 2014.
- Liu, Z., Mao, H., Wu, C.-Y., Feichtenhofer, C., Darrell, T., and Xie, S. A convnet for the 2020s. *arXiv preprint arXiv:2201.03545*, 2022.
- Long, J., Shelhamer, E., and Darrell, T. Fully convolutional networks for semantic segmentation. In *CVPR*, 2015.
- Loshchilov, I. and Hutter, F. Decoupled weight decay regularization. *arXiv preprint arXiv:1711.05101*, 2017.
- Meng, Y., Xiong, C., Bajaj, P., Tiwary, S., Bennett, P., Han, J., and Song, X. COCO-LM: Correcting and contrasting text sequences for language model pretraining. In *NeurIPS*, 2021.
- MMSegmentation. MMSegmentation: Openmmlab semantic segmentation toolbox and benchmark. <https://github.com/open-mmlab/mms Segmentation>, 2020.
- Paszke, A., Gross, S., Massa, F., Lerer, A., Bradbury, J., Chanan, G., Killeen, T., Lin, Z., Gimelshein, N., Antiga, L., Desmaison, A., Kopf, A., Yang, E., DeVito, Z., Raison, M., Tejani, A., Chilamkurthy, S., Steiner, B., Fang, L., Bai, J., and Chintala, S. Pytorch: An imperative style, high-performance deep learning library. In *NeurIPS*, 2019.
- Ramesh, A., Pavlov, M., Goh, G., Gray, S., Voss, C., Radford, A., Chen, M., and Sutskever, I. Zero-shot text-to-image generation. *arXiv preprint arXiv:2102.12092*, 2021.
- Rolfe, J. T. Discrete variational autoencoders. *arXiv preprint arXiv:1609.02200*, 2016.
- Srivastava, N., Hinton, G., Krizhevsky, A., Sutskever, I., and Salakhutdinov, R. Dropout: A simple way to prevent neural networks from overfitting. *JMLR*, 2014.
- Szegedy, C., Vanhoucke, V., Ioffe, S., Shlens, J., and Wojna, Z. Rethinking the inception architecture for computer vision. In *CVPR*, 2016.
- Touvron, H., Vedaldi, A., Douze, M., and Jégou, H. Fixing the train-test resolution discrepancy. *arXiv preprint arXiv:1906.06423*, 2019.
- Touvron, H., Cord, M., Douze, M., Massa, F., Sablayrolles, A., and Jégou, H. Training data-efficient image transformers & distillation through attention. In *ICML*, 2021a.
- Touvron, H., Cord, M., Sablayrolles, A., Synnaeve, G., and Jégou, H. Going deeper with image transformers. *arXiv preprint arXiv:2103.17239*, 2021b.
- Van Den Oord, A., Vinyals, O., et al. Neural discrete representation learning. In *NeurIPS*, 2017.
- Vaswani, A., Shazeer, N., Parmar, N., Uszkoreit, J., Jones, L., Gomez, A. N., Kaiser, Ł., and Polosukhin, I. Attention is all you need. In *NeurIPS*, 2017.

- Wei, C., Fan, H., Xie, S., Wu, C.-Y., Yuille, A., and Feichtenhofer, C. Masked feature prediction for self-supervised visual pre-training. *arXiv preprint arXiv:2112.09133*, 2021.
- Wightman, R., Touvron, H., and Jégou, H. Resnet strikes back: An improved training procedure in timm. *arXiv preprint arXiv:2110.00476*, 2021.
- Xie, Z., Zhang, Z., Cao, Y., Lin, Y., Bao, J., Yao, Z., Dai, Q., and Hu, H. Simmim: A simple framework for masked image modeling. *arXiv preprint arXiv:2111.09886*, 2021.
- Yu, J., Li, X., Koh, J. Y., Zhang, H., Pang, R., Qin, J., Ku, A., Xu, Y., Baldrige, J., and Wu, Y. Vector-quantized image modeling with improved vqgan. *arXiv preprint arXiv:2110.04627*, 2021.
- Yun, S., Han, D., Oh, S. J., Chun, S., Choe, J., and Yoo, Y. Cutmix: Regularization strategy to train strong classifiers with localizable features. In *ICCV*, 2019.
- Zhang, H., Cisse, M., Dauphin, Y. N., and Lopez-Paz, D. mixup: Beyond empirical risk minimization. *arXiv preprint arXiv:1710.09412*, 2017a.
- Zhang, K., Zuo, W., Chen, Y., Meng, D., and Zhang, L. Beyond a gaussian denoiser: Residual learning of deep cnn for image denoising. *TIP*, 2017b.
- Zhong, Z., Zheng, L., Kang, G., Li, S., and Yang, Y. Random erasing data augmentation. In *AAAI*, 2020.
- Zhou, B., Zhao, H., Puig, X., Xiao, T., Fidler, S., Barriuso, A., and Torralba, A. Semantic understanding of scenes through the ade20k dataset. *IJCV*, 2019.
- Zhou, J., Wei, C., Wang, H., Shen, W., Xie, C., Yuille, A., and Kong, T. ibot: Image bert pre-training with online tokenizer. *arXiv preprint arXiv:2111.07832*, 2021.

A. Appendix

A.1. The ImageNet-1K CIM Pre-training Configurations for Vanilla ViT and ResNet Models

Pre-training Config. (ViT & ResNet)	Value
Optimizer	AdamW (Loshchilov & Hutter, 2017)
Pre-training Epochs	300
Peak Learning Rate	1.5e-3
Batch Size	2048
Weight Decay	0.05
Optimizer Momentum (β_1, β_2)	(0.9, 0.98) (Vaswani et al., 2017)
Learning Rate Schedule	Cosine Decay
Gradient Clipping	3.0
Warmup Epochs	10
# Masked Patches for the Generator	100 to 120, Random Masking
The Generator’s Depth	4 to 6
The Generator’s Width	Same to the Enhancer (ViT), 384 (ResNet)
The Enhancer’s Loss Weight	1 for REVD _{ET} , 10 for RESPIX
Data Augmentation	RandomResizedCrop Only
Dropout (Srivastava et al., 2014)	\times
Stochastic Depth (Huang et al., 2016)	\times
LayerScale (Touvron et al., 2021b)	\times
Pos. Emb. in Transformer Layers	1-D Absolute Pos. Emb. (Dosovitskiy et al., 2020)
Patch Size	16
Pre-training Resolution	224

Table 9. The ImageNet-1K CIM pre-training settings for vanilla ViT-S/16, ViT-B/16 and ResNet-50 models. Notably, the pre-training configurations are almost the same for different architectures. We implement the pre-training using the codebase of BEiT (Bao et al., 2021). Mixed precision and deepspeed acceleration are used.

A.2. The ImageNet-1K Image Classification Fine-tuning Configurations for Vanilla ViT Models

Fine-tuning Config. (ViT)	Value
Optimizer	AdamW (Loshchilov & Hutter, 2017)
Fine-tuning Epochs	200 for ViT-S/16, 100 for ViT-B/16
Peak Learning Rate	3e-3 for ViT-B/16 RESPIX, 5e-3 for ViT-B/16 REVDet, 3e-3 or 4e-3 for ViT-S/16
Layer-wise Learning Rate Decay (Bao et al., 2021)	0.8 (Clark et al., 2020)
Batch Size	1024
Weight Decay	0.05
Optimizer Momentum (β_1, β_2)	(0.9, 0.999)
Learning Rate Schedule	Cosine Decay
Warmup Epochs	5
Gradient Clipping	X
Dropout (Srivastava et al., 2014)	X
Stochastic Depth (Huang et al., 2016)	0.1
Label Smoothing (Szegedy et al., 2016)	0.1
Mixup (Zhang et al., 2017a)	0.8
CutMix (Yun et al., 2019)	1.0
Random Augmentation (Cubuk et al., 2020)	9 / 0.5
Patch Size	16
Fine-tuning Resolution	224
Test Resolution	224
Test Crop Ratio	0.95
Loss Function	Cross Entropy Loss

Table 10. The ImageNet-1K image classification fine-tuning recipes for vanilla ViT-S/16 and ViT-B/16. We implement the fine-tuning using the codebase of BEiT (Bao et al., 2021). Mixed precision and deepspeed acceleration are used. We select the best learning rate out of {3e-3, 4e-3, 5e-3} for different sized models and pre-training objectives, and the absolute difference between the worst and the best learning rate is less than 0.3 in terms of the top-1 accuracy.

A.3. The ImageNet-1K Image Classification Fine-tuning Configurations for Vanilla ResNet-50

Fine-tuning Config. (ResNet-50)	100 Epoch FT	300 Epoch FT	600 Epoch FT
Optimizer	AdamW (Loshchilov & Hutter, 2017)		
Peak Learning Rate	12e-3		
Layer-wise Learning Rate Decay (Bao et al., 2021)	✗		
Batch Size	2048		
Learning Rate Schedule	Cosine Decay		
Loss Function	Binary Cross Entropy Loss		
Warmup Epochs	5		
Weight Decay	0.02	0.02	0.01
Fine-tuning Resolution	160	224	224
Test Resolution	224		
Test Crop Ratio	0.95		
Repeated Augmentation (Berman et al., 2019; Hoffer et al., 2019)	✗	✓	✓
Random Augmentation (Cubuk et al., 2020)	6 / 0.5	7 / 0.5	7 / 0.5
Mixup (Zhang et al., 2017a)	0.1	0.1	0.2
CutMix (Yun et al., 2019)	1.0		
Label Smoothing (Szegedy et al., 2016)	0.1	✗	0.1
Stochastic Depth (Huang et al., 2016)	✗	✗	0.05
Dropout (Srivastava et al., 2014)	✗		
Layer-wise Learning Rate Decay	✗		

Table 11. The ImageNet-1K image classification fine-tuning recipes for vanilla ResNet-50. We use the AdamW optimizer. The hyperparameter settings basically follows (Wightman et al., 2021). We implement the fine-tuning based on the codebase of BEiT (Bao et al., 2021). Mixed precision and deepspeed acceleration are used. For other self-supervised baseline approaches we compared in Table 2, we select the best learning rate out of {5e-3, 8e-3, 12e-3} and keep other settings unchanged.